Special Issue Research Article

Targeted Photodynamic Therapy of Human Head and Neck Squamous Cell Carcinoma with Anti-epidermal Growth Factor Receptor Antibody Cetuximab and Photosensitizer IR700DX in the Mouse Skin-fold Window Chamber Model[†]

Wei Peng[1,2,3]*, Henriette S. de Bruijn[2], Timo L. M. ten Hagen[4], Go M. van Dam[5], Jan L. N. Roodenburg[1], Kristian Berg[3], Max J. H. Witjes[1] and Dominic J. Robinson[2]

[1]Department of Oral and Maxillofacial Surgery, University Medical Center Groningen, Groningen, The Netherlands
[2]Centre for Optical Diagnostics and Therapy, Department of Otorhinolaryngology and Head & Neck Surgery, Erasmus University Medical Center Rotterdam, Rotterdam, The Netherlands
[3]Department of Radiation Biology, Institute for Cancer Research, Norwegian Radium Hospital, Oslo University Hospital, Oslo, Norway
[4]Laboratory of Experimental Oncology, Department of Pathology, Erasmus University Medical Center Rotterdam, Rotterdam, The Netherlands
[5]Department of Surgery, University Medical Center Groningen, Groningen, The Netherlands

ABSTRACT

Targeted photodynamic therapy (PDT) in head/neck cancer patients with a conjugate of the anti-epidermal growth factor receptor (EGFR) antibody, Cetuximab and a phthalocyanine photosensitizer IR700DX is under way, but the exact mechanisms of action are still not fully understood. In this study, the EGFR-overexpressing human head/neck OSC-19-luc2-cGFP tumor with transfected GFP gene was used in a skin-fold window chamber model in BALB/c nude mice. The uptake and localization of the conjugate in the tumor and its surrounding normal tissues were studied by an intravital confocal laser scanning microscopy with image analyses. The tumor was also irradiated with 690 nm laser light 24 h after conjugate administration. The vascular and tumor responses were examined by morphological evaluation and immunohistochemistry (IHC). The amount of conjugate in the tumor peaked at 24–48 h after injection. Image analyses of colocalization correlation parameters demonstrated a high fraction of the conjugate IR700DX colocalized in the GFP-expressing tumor cells. PDT-treated tumors showed extensive necrotic/apoptotic destruction with little vascular damage, while IHC showed no HIF-1α expression and decreased EGFR and Ki67 expression with activated caspase-3 overexpression, indicating a direct killing of tumor cells through both necrotic and apoptotic cell death.

INTRODUCTION

The worldwide incidence of head and neck cancers is estimated to be more than 550 000 each year with the mortality rate of about 300 000 (1,2). The tumors mainly arise from the squamous cell linings with more than 90% squamous cell carcinoma (3). Because of the complexity of the head and neck region with its critical structures, the treatment options do not only depend on the type and stage, but also the anatomic location of the tumor. The conventional treatment includes surgery or radiotherapy for early-stage I/II cancer (4–6), while combinations of surgery, radiotherapy and chemotherapy for advanced stage III/IV cancer (7–9). However, both surgery and radiotherapy often cause severe damage to surrounding normal tissues with a loss of their functions (10,11). Such morbidities have encouraged the field to search for new treatment alternatives for this disease.

The concept of photodynamic therapy (PDT) is attractive for cancer treatment (12–14) because the combination of a tumor-localizing photosensitizer with selective light delivery has the potential to provide a selective treatment for cancer with low morbidity (15). Effective PDT with the first generation photosensitizer such as hematoporphyrin derivative or porfimer sodium was shown in 1990s in the treatment of head and neck cancers (16), but prolonged skin photosensitivity with limited treatment depth of tumor (17,18) led investigators to look for second-generation photosensitizers with favorable properties of photochemistry, photophysics and photobiology (19,20). The European Medicines Agency (EMA)-approved PDT for palliative treatment of head and neck cancer with meta-tetra(hydroxyphenyl)chlorin (mTHPC, temoporfin) as a photosensitizer has shown to obtain complete response rates comparable to surgical treatment as well as to maintain good functional and cosmetic outcome in the treatment of squamous cell

carcinoma of the lip, oral cavity and pharynx (19,21,22). For larger lesions, surgery is more effective, but with the potential side effects of severe morbidities. Interstitial irradiation of temoporfin with its strong absorption of far-red wavelengths can enhance treatment depth, so that it may make it possible to treat larger tumors (23–25). However, the collateral phototoxicity of normal tissues to mTHPC-based PDT requires strict light protection protocols to prevent unwanted PDT effects. This has led to a search for alternative approaches that spare normal tissues.

Targeted PDT based on a photosensitizer linked to a targeting moiety with an affinity for tumor cells can improve the selective tumor distribution of the photosensitizer. Such targeting moieties include monoclonal antibodies, peptides, carbohydrates, folic acid and others (26). Epidermal growth factor (EGF), a protein produced in the body, attaches to its receptor (EGFR) of cells to trigger cellular proliferation. EGFR has been found to be over-expressed on the cell surface of several types of tumors including head and neck squamous cell carcinoma. Cetuximab, a chimeric (mouse/human) monoclonal antibody, is able to block the effect of EGF by binding EGFR, and was approved by EMA in 2004 and FDA in 2006 as a therapy for the treatment of patients with locally advanced squamous cell carcinoma of the head and neck in combination with radiation therapy (27). Phthalocyanines, a family of potent photosensitizers with their favorable properties of chemical stability, high fluorescence quantum yield and redshifted light absorption for optimal tissue penetration, have already been used for PDT of cancer patients in Russia (28). In general, hydrophilic phthalocyanines, such as IRDye700DX (IR700DX), have little photodynamic efficacy due to poor localization and are therefore commonly used to form a conjugate with a targeting moiety (29–31). IR700DX conjugated with an EGFR antibody has been shown to serve as both a diagnostic and a PDT-therapeutic agent (30,31). Based on a number of preclinical studies with promising results (31,32), a clinical trial with cetuximab and IR700DX was recently initiated by Rakuten Aspyrian, Inc. (https://clinicaltrials.gov/ct2/show/NCT02422979) (33) in patients with recurrent head and neck cancer. Although a rapid direct necrotic killing effect on tumor cells in vitro was noticed after the targeted PDT with IR700DX (31,32), the mode of cell death using this modality (including apoptosis) is still not fully understood. Further, the biological system of tumor cells cultured in vitro is significantly different from that of tumor tissue in vivo. Any antibody–dye conjugates including cetuximab/IR700DX go through the vascular system (including endothelium and tissues beneath its basal layer) and interstitial tissue space before reaching tumor cells in tumor tissue after systemic administration. Tumor destruction by a targeted PDT may thus involve direct and indirect (via initial vascular damage) killing effects on tumor cells that depend on the intratumoral localization of the conjugate. To better understand the correlation of kinetic uptake and localization patterns of such a conjugate in tumor with vascular and tumor responses after PDT, we have utilized intravital microscopy with window chamber technologies, such as the dorsal skin-fold, to image real-time dynamic processes in vivo (34–36). With this approach and using a mouse window chamber human head and neck OSC-19-luc2-cGFP tumor model in vivo with EGFR expression and transfected GFP genes, the aims of this study were to investigate (1) the kinetic patterns of the uptake and localization of the conjugate, cetuximab–IR700DX, in the tumor, (2) the vascular and tumor responses after the targeted PDT and (3) the

mechanisms of action of the targeted PDT on tumors with histopathology and immunohistochemistry.

MATERIALS AND METHODS

Human OSC-19-luc2-cGFP head and neck tumor cell line. The OSC-19-Luc2-cGFP (OSC-19) cell line was originally established in Japan from a patient with a well-differentiated squamous cell carcinoma of the tongue (37) and the OSC-19 cell line with transfected genes of luciferase 2 (luc2), and green fluorescent protein (GFP) was described previously (38). The cells were cultured in DMEM (Invitrogen, Carlsbad, CA) containing 4.5 g D-glucose L^{-1}, 110 mg L^{-1} sodium pyruvate L^{-1}, 580 mg L-glutamine L^{-1} supplemented with 10% FCS (Lonza, Basel, Switzerland), 100 IU mL^{-1} penicillin, 100 mg mL^{-1} streptomycin (Invitrogen), $1\times$ minimal essential medium (MEM) nonessential amino acids solution and $1\times$ MEM vitamin solution at 37°C in a humidified 5% CO_2 atmosphere. The passages of 10–40 of the cell line were used in this study.

Animals and skin-fold window chamber tumor model. An approval for the protocol of this study was obtained from the Erasmus University Medical Center and The Netherlands National Committee for the protection of animals used for scientific purposes. All experiments were conducted according to The National and European Ethical Committees' Guidelines on Animal Welfare. The skin-fold window chamber tumor model was made according to previously described procedures (36,39). Briefly, female BALB/c athymic nude mice from Janvier Labs (Saint-Berthevin Cedex, France) were 12 weeks old, weighed between 17 and 25 g, fed with chlorophyll-free complete food for 2 weeks prior to experiments and kept under specific pathogen-free conditions. After being anesthetized with inhalation of isoflurane/O_2, a dorsal skin flap of a mouse was made by dissecting the dorsal skin under aseptic conditions and a window chamber was then implanted on the dorsal skin flap. The OSC-19 cells had subcutaneously been inoculated into the dorsal skin flap (5×10^4 cells suspended in 10 μL serum-free medium) before a cover glass was placed to close the chamber. The window chamber was made of a synthetic material, polyether ether ketone (PEEK) that is inert and does not provoke immune reactions. The animals with the chamber were individually kept in a cage in a climate-controlled room with 32°C and 50%–60% humidity. The individual housing of mice prevents potential damage to the window chamber by other mice, while the high temperature and humidity avoid the cooling down and dehydration of the skin flap. Mice fitted with this chamber showed normal behaviors with
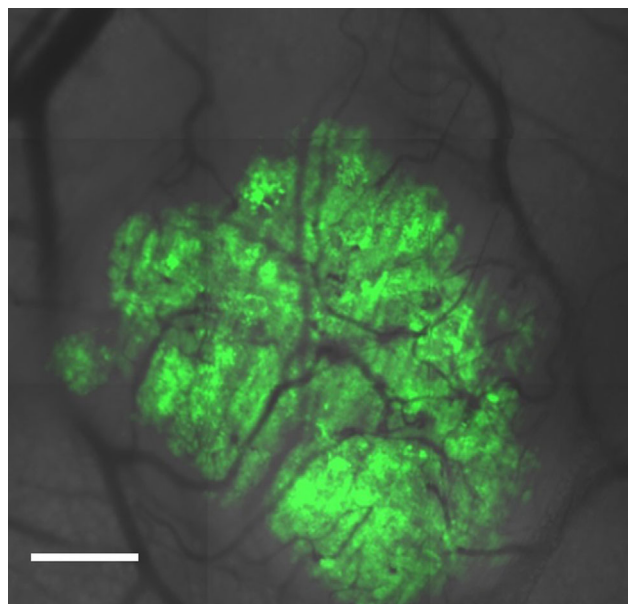

Figure 1. Microscopic green fluorescent protein (GFP)-expressing human head and neck OSC19 squamous cell carcinoma in a mouse skin-fold window chamber model. The image was made with the intravital LSM (bar: 500 μm). For the details, see the Section of Materials and Methods.

full capacity of motion and climbing. The general conditions of the window chamber together with tumor growth and its blood circulation were regularly checked by a confocal microscope at a low magnification to determine a best time to start the experiment with an average of 7 days after implantation of tumor cells (Fig. 1).

Intravital imaging. Experiments were started when the tumor showed microvascularization and growth (area: 0.5–2.5 mm^2). The animals ($n = 8$) were sedated with the inhalation of isoflurane/O$_2$ and placed on a 37°C temperature-controlled stage of a confocal microscope. The fluorescent tumor GFP (Ex/Em: 488/BP505–530 nm) and conjugate IR700DX (Ex/Em: 633/LP650 nm) in tumor and its surrounding normal tissues were optically sectioned to a 9 μm thickness and imaged by the Zeiss laser scanning microscope (LSM) 510–Axiovert 200M (Carl Zeiss, Thornwood, NY) with a 10× objective at 0, 4, 24 and 48 h after i.v. administration of the conjugate cetuximab–IR700DX (100 μL of 1 mg mL^{-1} from Rakuten Aspyrian Inc. San Diego, USA) via the tail vein. A mode of the system was set to enable the PC to control the microscope, xy-table, z-positioning and image capture with three detection channels of transmission, GFP and IR700DX. During the study period of 48 h, the animals were kept under reduced light conditions to avoid possible phototoxic effects of the conjugate, after which all animals were sacrificed by cervical dislocation.

Since one image made by the LSM system with a 10× objective cannot cover the field of a whole tumor and its surrounding normal tissues, nine images were acquired in each of the three channels to visualize an area large enough to include a tumor and its surrounding normal tissues. Based on the transmission and tumor GFP images, the areas of tumor, vessels and connective tissue were identified. At least three regions of interest were randomly chosen in the areas of each type of tissues for image analyses with *ImageJ* to study the kinetic uptake of the conjugate by tumor and its surrounding normal tissues.

For the colocalization study, a total of eight live mice with 1–3 tumors per mouse were used. Eight optically sectioned serial confocal fluorescent images (9 μm thickness) of conjugate IR700DX and eight corresponding tumor GFP images were acquired using the Zeiss LSM 510 with a 20× objective in each tumor at 0 and 4, 24 and 48 h after i.v. administration of conjugate via the tail vein. One of the eight conjugate IR700DX images, randomly chosen with its respective tumor GFP image, was used to carry out the colocalization image analyses with the *Fiji* software (http://fiji.sc) of the image processing program *ImageJ*. The background (including dark current of the microscopy) of the images of the tissue samples taken from the animals prior to the conjugate injection was subtracted. The coloc2 plugin in the *Fiji* version was used to calculate pixel-intensity correlation-based colocalization parameters of Pearson's R value (a measure of the strength of the linear relationship between two different types of fluorescent signal images) and Mander's tM1 parameter (a measure of the colocalization coefficient between two images).

Targeted PDT in four tumor-bearing animals was performed on the tumors under 690 nm laser irradiation (ML7700, Modulight, Inc., Finland) through a frontal light distributor (Medlight SA, Ecublens, Switzerland) to a dose of 100 J cm^{-2} (at 50 mW cm^{-2}) 24 h after conjugate administration. Normal and tumor vascular responses prior to and 5-min, 2, 24 and 48 h after light exposure were determined by transmission microscopy with a 10× objective (Leica SP5 AOBS Multiphoton lasers, Wetzlar, Germany). In addition, the fluorescent rhodamine dextran 2 MDa was immediately (<10 min) imaged after its i.v. administration (100 μL of 1 mg mL^{-1}) with the same microscopic system (Ex/Em: 555/580 nm) to study vascular leakage in the tumor and surrounding normal tissues at 2 h after targeted PDT.

Histopathology and immunohistochemistry (IHC). The destructive effects of the targeted PDT on two of the four tumors were examined by histopathological evaluation and IHC. The other two tumors were too small to be used for such study. Three untreated tumors were also included as controls. Normal and tumor tissues of the skin-fold window chamber were harvested at 48 h after the targeted PDT, immediately frozen in liquid nitrogen and stored in −80°C before use. The tissues were fixed in a 10% buffered formalin solution and paraffin-embedded. Three μm tissue sections were then made and stained with hematoxylin and eosin (H&E). In addition, the sections were immunostained using the Dako EnVision + system (K8012, Dako Cooperation, CA, USA) and Dako Autostainer. Deparaffinization, rehydration and target retrieval were performed in a Dako proteinase K (for EGFR) or a Dako PT-link (for hypoxia-inducible factor 1-alpha (HIF-1a), Ki67, cleaved caspase-3 and LC3) and EnVision Flex target retrieval solution. Endogenous peroxidase

was blocked using a Dako blocking reagent for 5 min followed by incubation at 4°C over night with primary antibody against EGFR (mouse monoclonal antibody, Clone H11, 1:200 dilution, Dako Corporation, CA, USA) and at room temperature for 30 min with primary antibodies against HIF-1a (rabbit polyclonal antibody, 1:300 dilution, Novus Europe, UK), Ki67 (mouse monoclonal antibody, Clone MIB-1, 1:150 dilution, DakoCytomation, Denmark A/S), cleaved caspase-3 (rabbit polyclonal antibody, 1:100 dilution, Novus Europe, UK) and LC3 (#2775, 1:1000 dilution, Cell Signaling, The Netherlands). Thereafter, the sections were incubated with a Dako EnVision FLEX + mouse or rabbit linker for 15 min followed by incubation with Dako EnVision FLEX/horseradish peroxidase for an additional 30 min. For visualization of staining, the sections were treated with 3′3-diaminobenzidine tetra-hydrochloride (DAB) for 10 min, counterstained with hematoxylin and mounted in a toluene-free mounting medium (Dako, Danmark A/S).

Statistical analysis. Student's *t*-test was used to analyze differences in the fluorescence intensities of the conjugate in tumor and normal tissues. The same test was also employed to analyze the colocalization data obtained from *ImageJ*. A $P < 0.05$ value was considered to be statistically significant.

RESULTS

Uptake, localization and colocalization of the conjugate in tumor

Figure 2 shows an example of transmission, GFP and IR700DX images that were used to quantify the uptake of conjugate by tumor and its surrounding normal tissues. The red fluorescent IR700DX of the conjugate was already seen in the tumor and its surrounding vessels (arrow in Fig. 2) with some vascular branches in the tumor areas at 4 h after its administration. At 24 and 48 h, more conjugate was distributed in the tumor with little in the vessels (arrows in Fig. 2). Quantitative measurements with image analyses demonstrate that the conjugate in the tumor tissue increased with times after i.v. injection with a peak at 24–48 h and was significantly higher than that in the surrounding blood vessels and normal connective tissue ($P < 0.05$; Fig. 3).

Figure 4 shows a negative value of Pearson's R value in the samples taken before conjugate injection. At 4 h after conjugate injection, very low values of Pearson's R value were seen between the conjugate IR700DX and tumor GFP. The analyses of the images taken at 24 and 48 h after conjugate injection show higher values of the correlation parameter (Fig. 4), demonstrating a higher degree of colocalization of the two different fluorescent signals. Furthermore, high values of Mander's tM1 at all time points illustrate that the fraction of conjugate IR700DX was largely colocalized with the tumor GFP areas (Fig. 4). Statistically, Pearson's R value shows a significant difference between 4 and 24 h ($P = 0.002$) with no significant difference between 24 and 48 h ($P = 0.153$). These statistical data may indicate a significant difference between 4 and 24–48 h in terms of the degree of pixel-intensity correlation of conjugate IR700DX and tumor GFP. However, the statistical analyses of Mander's tM1 show no significant difference between 4 and 24–48, suggesting a high degree of colocalization correlation of the two different signals between the different time points.

Vascular responses to targeted PDT

Four animals with the skin-fold window chamber tumor model were used to study normal and tumor vascular responses in real-time during targeted PDT (Fig. 5). The extent of the vascular responses was also semiquantified and presented in the Table 1. No changes in the large blood vessels in normal tissue around tumors were seen at 5 min after targeted PDT in two out of four
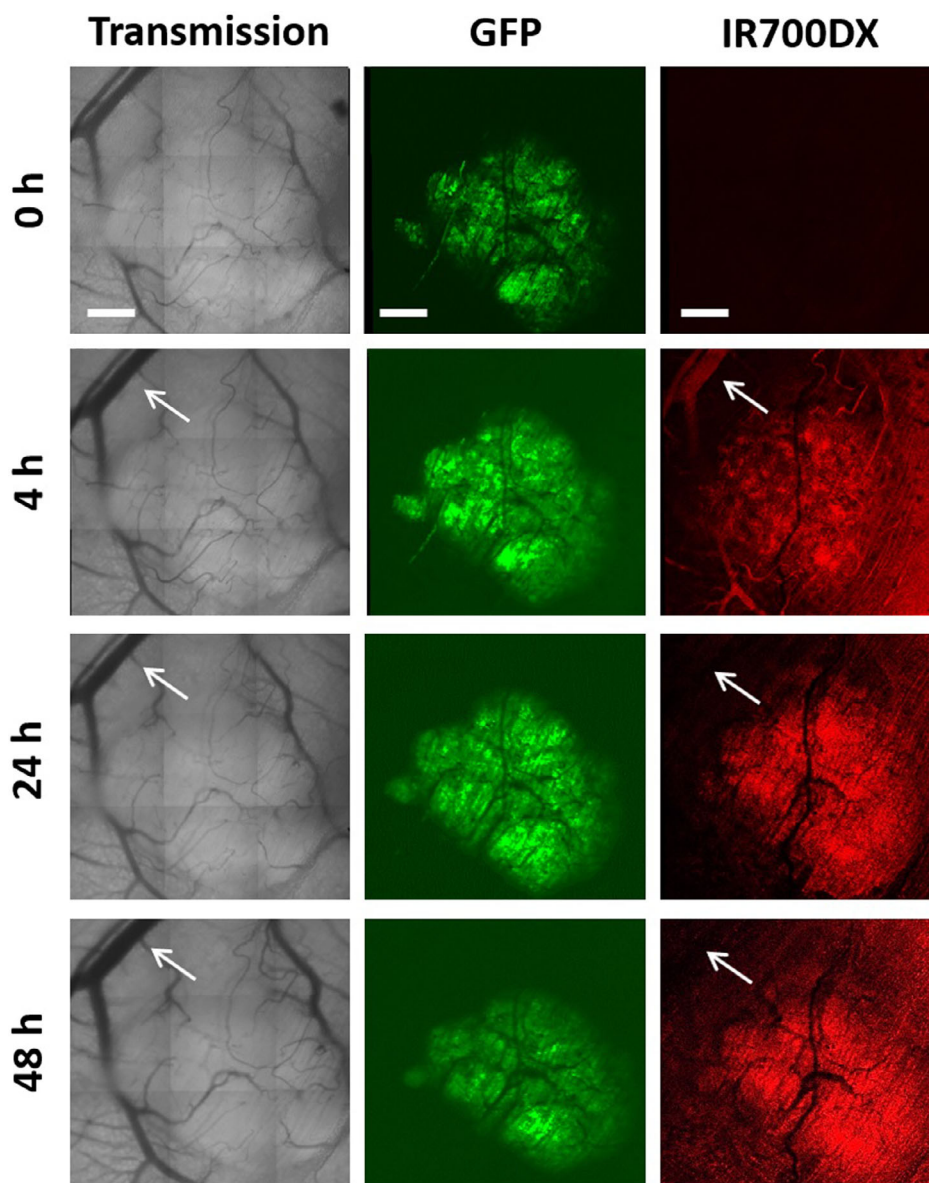
Figure 2. Kinetic localization patterns of the cetuximab–IR700DX conjugate in the OSC19 tumor and its surrounding normal tissues in the skin-fold window chamber at 0, 4, 24 and 48 h after i.v. injection. The images were obtained from one of the tumors examined including transmission, green tumor GFP signals and red cetuximab–IR700DX conjugate together with arrows for the blood vessels in the surrounding normal tissue. The images were acquired with the intravital LSM (bars: 500 μm). For the details, see the Section of Materials and Methods.

animals (T-1 & T-2), but the vessels were slightly constricted at 2 h and severely contracted at 24 h. At 48 h after targeted PDT, the function of all vessels had recovered with visible blood flow in the two animals (Fig. 5, Table 1). In the third animal, a slight constriction of the large blood vessels was observed at 5 min after targeted PDT followed by apparent dilatation of the vessels at 2 h before the recovery of their function at 24 h (Fig. 5, Table 1). Similarly, the large vessels were dilated at 2 h after PDT in the fourth animal with a recovery at 24 h (Fig. 5, Table 1). No permanent damage to the large blood vessels was observed at 48 h after PDT in all the four animals (Fig. 5). Furthermore, the vascular responses in the four animals were determined by imaging rhodamine dextran 2 MDa extravasation at 2 h after targeted PDT. Figure 6 shows no leakage of rhodamine dextran 2 MDa in all

the four tumors, indicating that the targeted PDT does not cause a severe damage to tumor vascular structures. However, there was some Rhodamine leakage in the tumor-surrounding normal tissues (red regions highlighted in Fig. 6).

Tumor destruction by targeted PDT

The tumor tissue response to the targeted PDT was examined by histopathology and IHC. Untreated tumors in the skin-fold window chamber demonstrate viable tumor cells with no damaged alterations by histopathology with H.E. staining (Control in Fig. 7). IHC of the control tumors showed homogenous cell surface expression of EGFR and nuclear staining of the proliferative factor Ki67 in individual tumor cells (Fig. 7). In addition, some
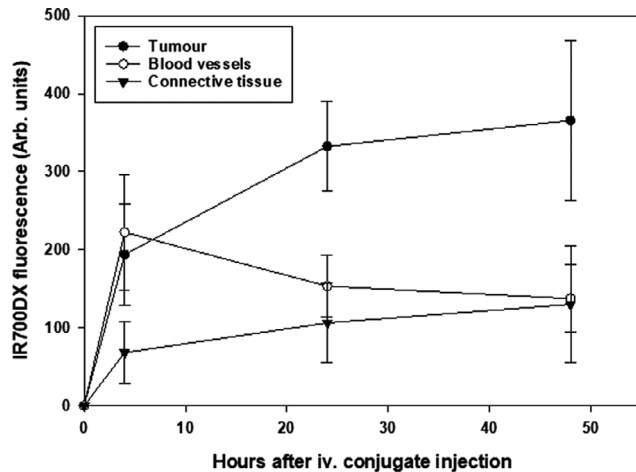
Figure 3. Kinetic patterns of uptake of the cetuximab–IR700DX conjugate by the OSC19 tumor and its surrounding normal blood vessels and connective tissue in the skin-fold window chamber at various times after i.v. injection. The amounts of the conjugate in the tissues were measured by quantifying the fluorescent signals of the conjugate IR700DX with the intravital LSM as described in the Section of Materials and Methods.

positive cleaved caspase-3 cells were seen (Fig. 7). The tumors treated with the targeted PDT have shown an extensive damage with necrotic and apoptotic (nuclear condensation) cell death (H.E. in Fig. 7). Some slight damage in the overlying normal skin tissue was also seen (Fig. 7). In addition, inhomogenous, weak staining of EGFR and of the proliferative factor, Ki67 suggests a decreased expression of EGFR and Ki67 in tumor cells. Moreover, the cleaved caspase-3, a pivotal factor for the execution of cell apoptosis, was apparently overexpressed in the tumor cells, indicating apoptotic cell death after the targeted PDT (Fig. 7). LC3, a central protein in the autophagy pathway and a marker of autophagosomes, was not expressed (data not shown), suggesting no involvement of autophagy in the tumor cell death. Interestingly, no congestion and hemorrhage of blood vessels were seen in the tumors and surrounding normal tissues (Fig. 8).

IHC showed typical brownish nuclei of positive staining of HIF-1a, a well-known transcription factor for regulating cellular response to hypoxia, in the epidermal cells, but not in the beneath tumor cells (Fig. 8). This was consistent with no severe vascular damage demonstrating that the tumor destruction by the targeted PDT was largely due to a direct killing effect rather than an indirect effect via vascular damage.

DISCUSSION

A dorsal skin-fold window chamber tumor model in combination with confocal imaging technologies can offer a unique opportunity to quantitatively analyze in real-time the fluorescence-based pharmacokinetics and biodistribution of the cetuximab/IR700DX conjugate in the OSC-19 tumor and its surrounding normal tissues in living athymic mice. In addition, this technique can visualize the dynamic patterns of normal and tumor vascular responses to the targeted PDT. Such studies would help to optimize parameters affecting the targeted PDT efficacy. Cetuximab/IR700DX was taken up by the tumor cells already at 4 h and peaked at 24 and 48 h after administration. It was still detectable in the blood at 4 h after administration and less at later time points. A 24 h drug–light interval was therefore chosen for the subsequent targeted PDT of the tumor in this study. The same interval is also being used in the ongoing clinical trial of the targeted PDT in head and neck cancer patients. While cetuximab is a chimeric (mouse/human) antibody against human EGFR, it does not bind to mouse EGFR. The increase in fluorescence in normal mouse tissues observed in this model is likely to be the result of content in the blood circulation and unspecific uptake of the conjugate. It should be mentioned that IR700DX in a free form was not included in this study because this water-soluble dye has been shown in several reports to be little taken up by tumor tissues with little subsequent photodynamic effects (29–31,40).

The microscopy-based methods to study colocalization of markers in biological systems are often qualitatively descriptive rather than quantitative. For example, to overlap a green and a red fluorescent images for two various markers with a resultant
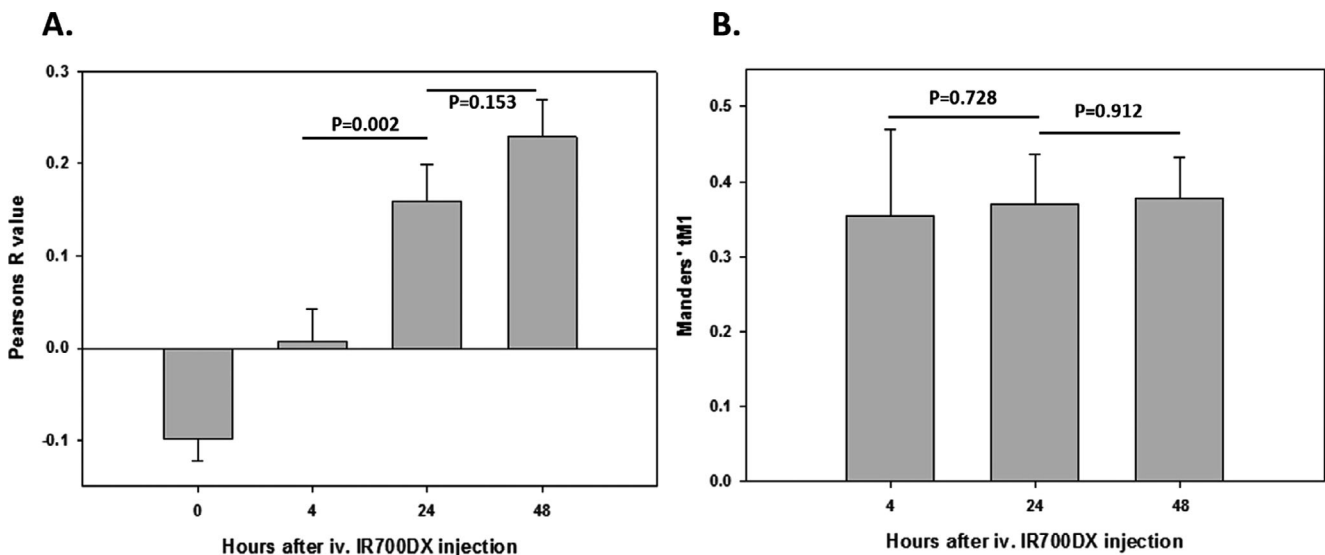

Figure 4. Image analyses of the colocalization correlation parameters of (A) Pearson's R value and (B) Manders' tM1 for the conjugate IR700DX and tumor GFP using the coloc2 plugin of ImageJ. Zero hour in the plots is prior to the conjugate administration. The background of the 0 h images is subtracted in Manders' tM1 plot.
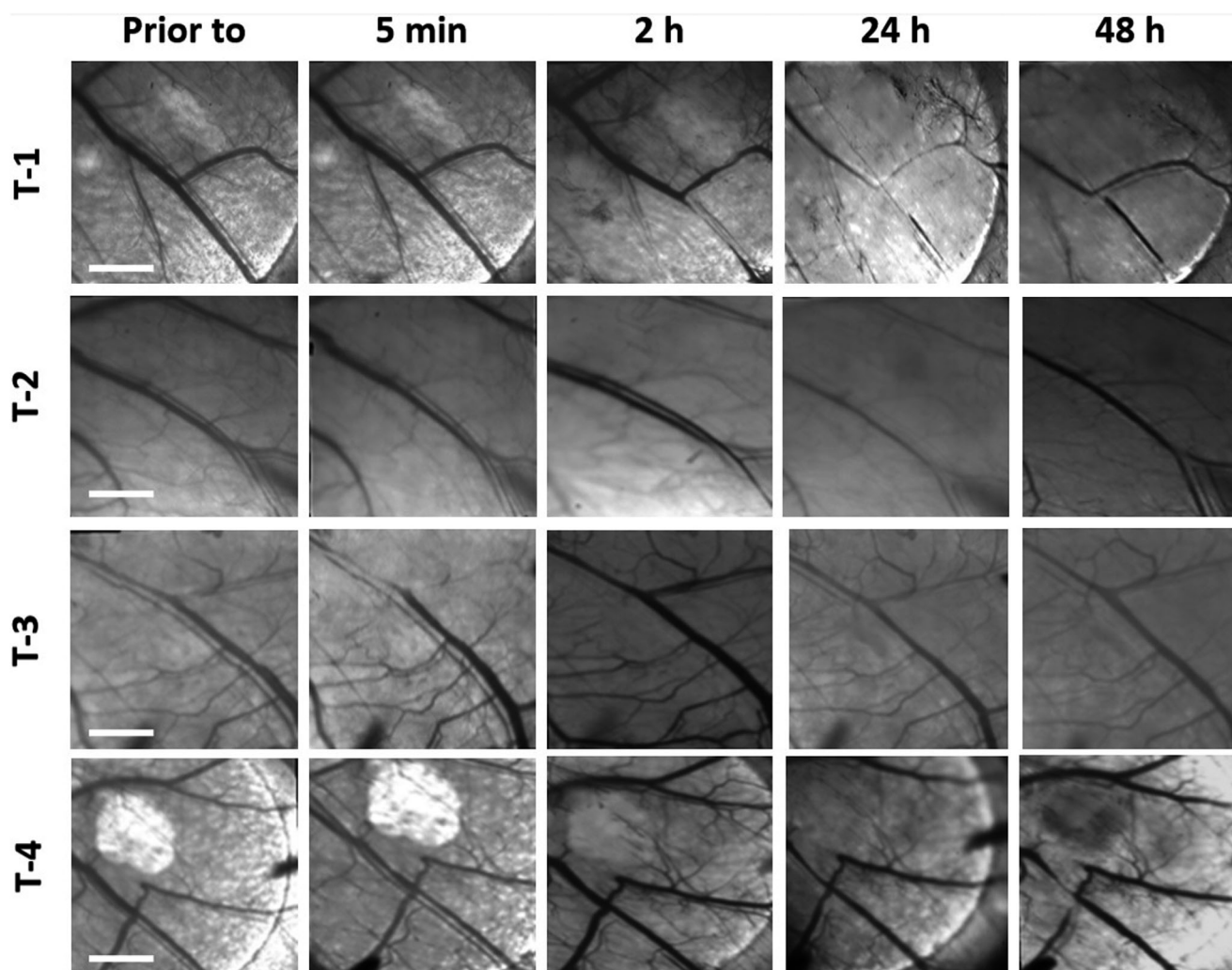
Figure 5. Kinetic changes of vascular responses of four treated tumor-bearing animals in the window chamber were determined by the intravital transmission LSM at prior to and 5 min, 2, 24 and 48 h after the targeted PDT (bars: 2000 μm). For the details, see the Section of Materials and Methods.

Table 1. Vascular responses to targeted PDT.

Tumors	Prior to	5 min	2 h	24 h	48 h
Tumor-1	−	−	+	++	−
Tumor-2	−	−	+	++	−
Tumor-3	−	+	+	−	−
Tumor-4	−	−	+	−	−

EGFR-overexpressing human head and neck OSC-19-luc2-cGFP tumor in the mouse skin-fold window chamber was irradiated with a 690 nm laser at a dose of 100 J cm^{-2} (50 mW cm^{-2}) at 24 h after the i.v. injection of Cetuximab-IR700DX conjugate. The vascular responses were semiquantified by (−) no changes in the vascular lumen with normal blood flow, (+) slight changes in narrowing or dilating the vascular lumen, but still with visible blood flow and (++) severely changes in narrowing the vascular lumen and/or shutting down the vessels with no detectable blood flow.

yellow color image is still commonly used to assess colocalization. However, such a visual estimation does not allow quantification of the degree of colocalization. Based on the initial work by Pearson in 1896 (41), several statistical methods of pixel-intensity correlation have been developed to quantify the degree of colocalization of two fluorescence channels (42,43). The significant lower level of Pearson's R value at 4 h than 24 h (Fig. 4) is in agreement with the pixel-intensity-based "uptake" data with a lower amount of IR700DX in the tumors at 4 h than 24–48 h (Fig. 3). Further, the relative high values of Manders' tM1 as a colocalization quantifier demonstrate a high fraction of positive IP700DX areas that colocalizes with the tumor GFP. No significant difference of Mander's tM1 in the images taken at 4, 24 and 48 h suggests that IR700DX was localized in the tumor cells with a relative high specificity during the study period.

Microvascular structures of a tumor are usually vulnerable to PDT. This starts with recoverable functional disturbance, such as vasoconstriction and vasodilatation, in the arterioles, capillaries and postcapillary venules. This often results in aggregation of blood cells and thereby reduced blood flow and possibly finally complete stasis (44–46). The vasoconstriction may be caused by the release of thromboxane, a potent vasoconstrictor formed from damaged cell membrane lipids such as from platelets (47). Conversely, histamine, a powerful vasodilator released from the degranulation of mast cells, may induce the vasodilatation (48). Furthermore, if a photosensitizer is localized in the collagen
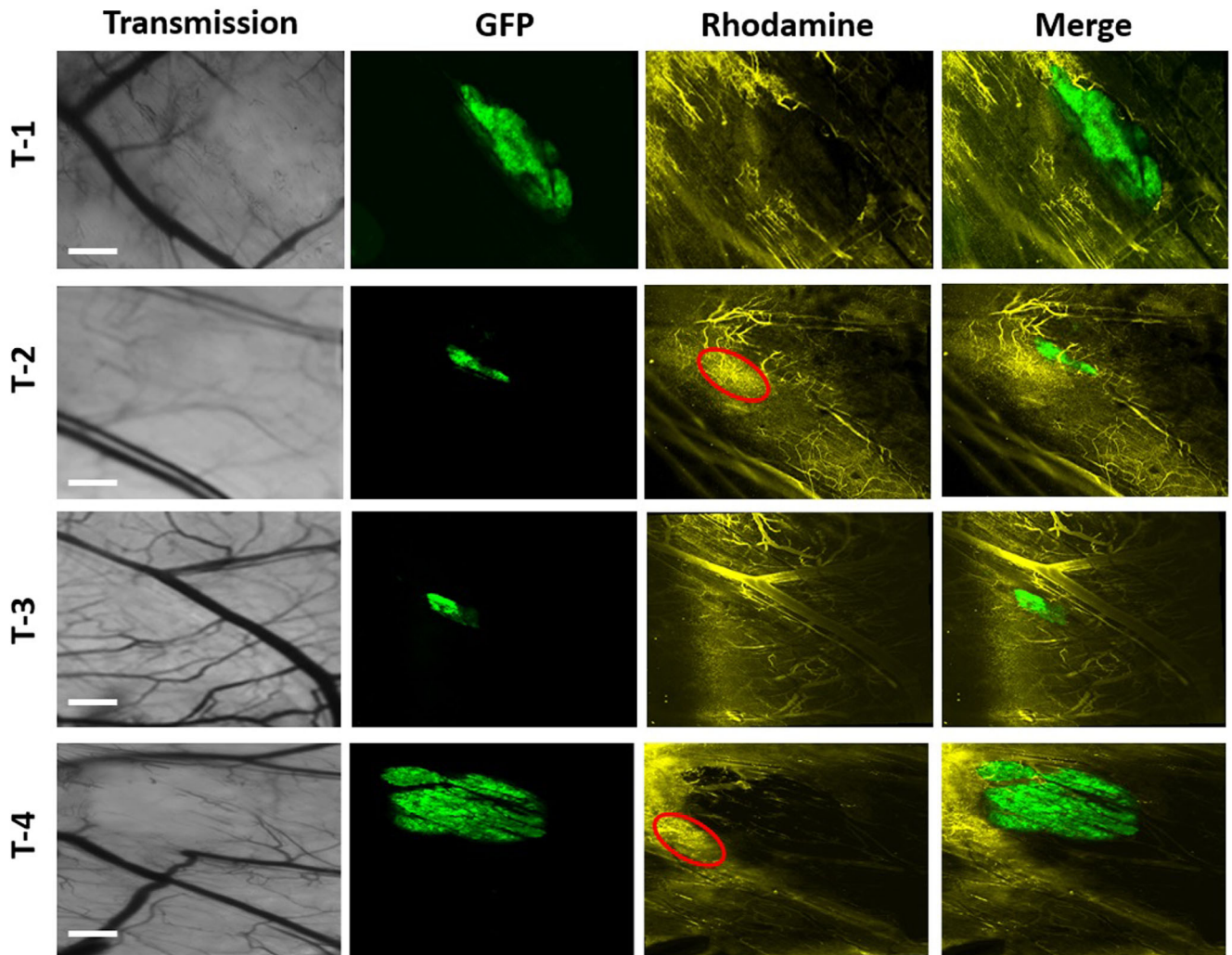
Figure 6. The fluorescent rhodamine dextran 2 MDa was imaged immediately after its i.v. injection as a marker for vascular leakage in four tumor-bearing animals at 2 h after the targeted PDT. The images were acquired with the intravital LSM including transmission, green tumor GFP, yellow rhodamine dextran 2MDa and merge of GFP and Rhodamine (bars: 1000 μm). For the details, see the Section of Materials and Methods. The red regions in the T-2 and T-4 indicate some leakage of rhodamine dextran 2 MDa from the normal vessels around the tumors.

fibers and connective tissue elements of the subendothelial zone of the capillary wall, this may lead to permanent vascular damage after light activation. No permanent vascular damage in this study suggests that the targeted PDT may not damage the subendothelial zone of the vasculature. Normally, the effects of hypoxia/anoxia on tumor due to functional alterations of vessels are limited if they do not last for a long time, as an effective PDT usually requires a permanent vascular damage (49). The initial mild to severe constriction followed by dilation of the vascular responses was observed up to 24 h after the targeted PDT in the present study. This might be due to a nonspecific photodynamic effect of circulating conjugates on the vascular walls, since some conjugate in the blood vessels was still seen at 24 h after injection (Fig. 3). Such microvascular effects were not permanent, as the vascular functions were recovered at 48 h after the targeted PDT. Moreover, the rhodamine dextran 2 MDa extravasation confirmed no leakage of the tumor vessels, suggesting no structural damage of the tumor vessels. Consistently, no expression of HIF-1α in the tumor cells (Fig. 8) indicates that the targeted

PDT-induced transient vascular alterations did not result in a severe hypoxic condition in the tumors.

Histopathology and IHC demonstrate an extensive necrotic destruction of the two tumors 48 h after the targeted PDT with no signs of hemorrhage. Thus, such tumor damage may not involve the blood vessels. Only slight damage of the overlying epidermis was observed, most likely the result of unspecific uptake of the conjugate. The binding of the conjugate to the EGFR of the OSC-19 tumor cells most likely played a crucial role in the direct killing of tumor cells by the targeted PDT.

EGF, a small mitogenic protein, binds to EGFR on the cell surface to induce autophosphorylation of several tyrosine residues in the C-terminal domain of EGFR. This leads to a stimulation of its intrinsic tyrosine kinase activity. It is well known that overexpression of EGFR promotes cell cycle progression from the G1 to S phase to increase cell proliferation. In this study, the down-expression of EGFR with downregulation of the proliferative factor Ki67 of the tumor cells as seen by IHC supports the tumor damage via targeting EGFR of the targeted PDT.
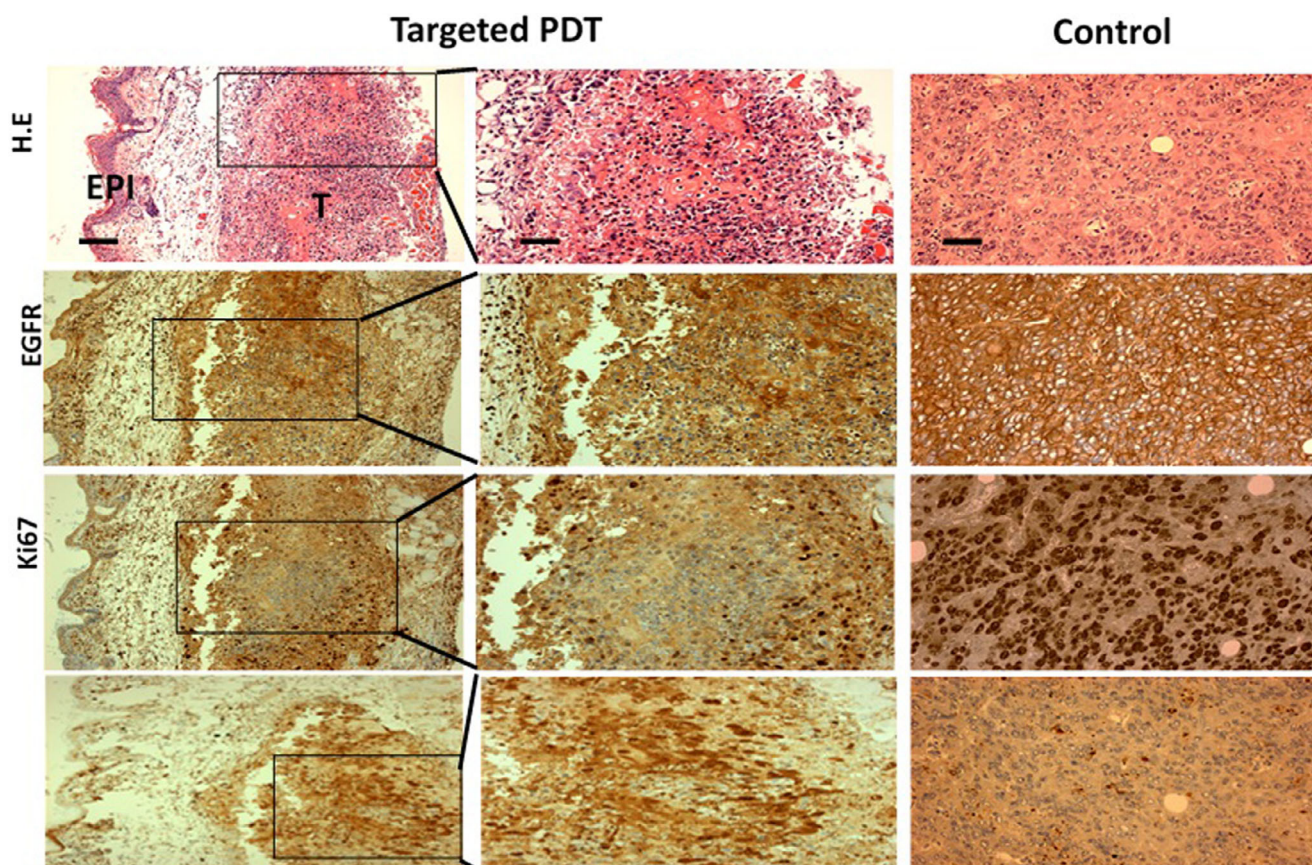
Figure 7. Hematoxylin–eosin (H.E.) staining and immunohistochemistry of EGFR, Ki67 and cleaved caspase-3 of tumors at 48 h after the targeted PDT (the bars in H.E. images: 100 µm for the left column of images and 50 µm for the middle column of images). EPI, epidermis; T, tumor. A control tumor is also included (the bar in the H.E. image is 50 µm for the right column of images).
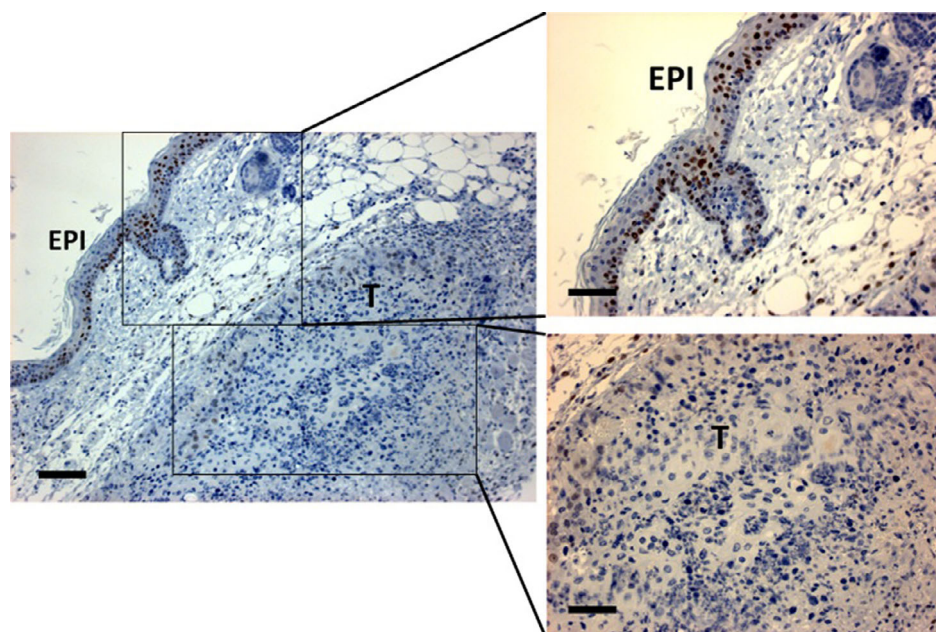

Figure 8. Immunohistochemistry of HIF-1α in a tumor at 48 h after the targeted PDT. EPI, epidermis; T, tumor. Epidermal cells show HIF-1a staining of brownish nuclei served as "internal" positive controls, while no HIF-1α is seen in the subcutaneous tumor cells. The bars: 100 µm for the left image and 50 µm for the right images.

Since the first report by Agarwal et al. in 1991 on the apoptotic induction by PDT with chloroaluminium phthalocyanine (50), a large number of studies have concluded that PDT can induce cell death through apoptosis. Apoptosis, or programmed cell death, is a form of cell death distinct from necrosis with respect to the characteristics of morphology and biochemistry. Cytosolic aspartate-specific (cysteine) proteases, called caspases, are responsible for the induction of apoptosis. All apoptotic caspases exist in cells as an inactive form. When cells undergo apoptosis, these caspases become activated through one or more sequential proteolytic events that cleave the single peptide precursor into large and small fragments. Among them, the caspase-8, caspase-9 and caspase-3 appear to play a crucial role in the degradative events in apoptosis. Currently, there are two well-characterized pathways of caspase-activating cascades that regulate apoptosis: the cell surface death receptor pathway via cleavage of caspase-8 and the mitochondrial-initiated pathway via cleavage of caspase-9. The cleaved caspase-8 or caspase-9 then activates the downstream executioner, caspase-3. The nuclear condensation of some tumor cells with the upregulation of cleaved caspase-3 in this study suggests an apoptotic induction probably through a receptor-mediated pathway after directly targeting EGFR by the targeted PDT. No positive detection of the LC-3 as a marker of autophagy may indicate no involvement of the autophagic process in this study.

CONCLUSIONS

The fluorescent kinetic uptake and localization patterns of the cetuximab/IR700DX conjugate in the EGFR-overexpressing human head and neck OSC-19 tumors in the mouse skin-fold window chamber were studied in real-time. The amounts of the conjugate peaked at 24–48 h in the tumor tissue. The light exposure then caused initial contraction and subsequent dilatation of the normal blood vessels followed by functional recovery at 48 h. No leakage of the rhodamine dextran 2 MDa within the tumor tissue, together with negative staining of HIF-1α in the tumor cells by IHC, suggests no substantial damage to the tumor vascular structure, neither a severe hypoxic condition in the tumors after the targeted PDT. Furthermore, the extensive tumor necrosis shown by histopathology with H.E. staining and the cleavage of caspase-3 by IHC in the tumor cells demonstrates both necrotic and apoptotic cell deaths are involved in the tumor destruction. These results suggest that such an effective modality was largely due to a direct effect on the EGFR-overexpressing OSC-19 tumor cells via the specific light-activated cetuximab–IR700DX conjugate rather than an indirect effect from vascular damage. This study demonstrates that targeted PDT with the cetuximab/IR700DX conjugate may have a potential for treating EGFR expressing tumors.

REFERENCES

1. Jemal, A., F. Bray, M. M. Center, J. Ferlay, E. Ward and D. Forman (2011) Global cancer statistics. *CA Cancer J. Clin.* **61**, 69–90.
2. HEAD and NECK Cancer (2014) Union for International Cancer Control. Review of Cancer Medicines on the WHO List of Essential Medicines.
3. Vigneswaran, N. and M. D. Williams (2014) Epidemiologic trends in head and neck cancer and aids in diagnosis. *Oral Maxillofac. Surg. Clin. North Am.* **26**, 123–141.
4. Wolfensberger, M., P. Zbaeren, P. Dulguerov, W. Muller, A. Arnoux and S. Schmid (2001) Surgical treatment of early oral carcinoma-results of a prospective controlled multicenter study. *Head Neck* **23**, 525–530.
5. Argiris, A., M. V. Karamouzis, D. Raben and R. L. Ferris (2008) Head and neck cancer. *Lancet* **371**, 1695–1709.
6. Bhalavat, R. I., U. M. Mahantshetty, S. Tole and S. V. Jamema (2009) Treatment outcome with low-dose-rate interstitial brachytherapy in early-stage oral tongue cancers. *J. Cancer Res. Ther.* **5**, 192–197.
7. Cohen, E. E., M. W. Lingen and E. E. Vokes (2004) The expanding role of systemic therapy in head and neck cancer. *J. Clin. Oncol.* **22**, 1743–1752.
8. Haddad, R. I. and D. M. Shin (2008) Recent advances in head and neck cancer. *N. Engl. J. Med.* **359**, 1143–1154.
9. Pignon, J. P., A. le Maitre, E. Maillard and J. Bourhis (2009) MACH-NC Collaborative Group. Meta-analysis of chemotherapy in head and neck cancer (MACH-NC): an update on 93 randomised trials and 17,346 patients. *Radiother. Oncol.* **92**, 4–14.
10. Finlay, P. M., A. G. Dawson and D. S. Soutar (1992) An evaluation of functional outcome after surgery and radiotherapy for intraoral cancer. *Br. J. Oral. Maxillofac. Surg.* **30**, 14–17.
11. Bundgaard, T., O. Tandrup and O. Elbrond (1993) A functional evaluation of patients treated for oral cancer. A prospective study. *Int. J. Oral. Maxillofac. Surg.* **22**, 28–34.
12. Dolmans, D. E., D. Fukumura and R. K. Jain (2003) Photodynamic therapy for cancer. *Nat. Rev. Cancer* **3**, 389–387.
13. Agostinis, P., K. Berg, K. A. Cengel, T. H. Foster, A. W. Girotti, S. O. Gollnick, S. M. Hahn, M. R. Hamblin, A. Juzeniene, D. Kessel, M. Korbelik, J. Moan, P. Mroz, D. Nowis, J. Piette, B. C. Wilson and J. Golab (2011) Photodynamic therapy of cancer: an update. *CA Cancer J. Clin.* **61**, 250–281.
14. van Straten, D. V., H. S. de Mashayekhi, S. O. Bruijn and D. J. Robinson (2017) Oncologic photodynamic therapy: basic principles, current clinical status and future directions. *Cancers (Basel)* **9**, 19.
15. Marchal, S., G. Dolivet, H. P. Lassalle, F. Guillemin and L. Bezdetnaya (2015) Targeted photodynamic therapy in head and neck squamous cell carcinoma: heading into the future. *Lasers Med. Sci.* **30**, 2381–2387.
16. Feyh, J. (1996) Photodynamic treatment for cancers of the head and neck. *J. Photochem. Photobiol B.* **36**, 175–177.
17. Biel, M. A. (2010) Photodynamic therapy of head and neck cancers. *Methods Mol. Biol.* **635**, 281–293.
18. Ikeda, H., T. Tobita, S. Ohba, M. Uehara and I. Asahina (2013) Treatment outcome of photofrin-based photodynamic therapy for T1 and T2 oral squamous cell carcinoma and dysplasia. *Photodiagn. Photodyn. Ther.* **10**, 229–235.
19. de Visscher, S. A. H. J., P. U. Dijkstra, I. B. Tan, J. L. N. Roodenburg and M. J. H. Witjes (2013) mTHPC mediated photodynamic therapy (PDT) of squamous cell carcinoma in the head and neck: a systematic review. *Oral Oncol.* **49**, 192–210.
20. Meulemans, J., P. Delaere and V. Vander Poorten (2019) Photodynamic therapy in head and neck cancer: indications, outcomes, and future prospects. *Curr. Opin. Otolaryngol. Head Neck Surg.* **27**, 136–141.
21. Kubler, A. C., J. de Carpentier, C. Hopper, A. G. Leonard and G. Putnam (2001) Treatment of squamous cell carcinoma of the lip using Foscan-mediated photodynamic therapy. *Int. J. Oral Maxillofac. Surg.* **30**, 504–509.
22. Copper, M. P., I. B. Tan, H. Oppelaar, M. C. Ruevekamp and F. A. Stewart (2003) Meta-tetra(hydroxyphenyl)chlorin photodynamic therapy in early-stage squamous cell carcinoma of the head and neck. *Arch. Otolaryngol. Head Neck Surg.* **129**, 709–711.
23. Hopper, C. (2000) Photodynamic therapy: a clinical reality in the treatment of cancer. *Lancet Oncol.* **1**, 212–219.
24. Tan, I. B., G. Dolivet, P. Ceruse, V. Vander Poorten, G. Roest and W. Rauschning (2010) Temoporfin-mediated photodynamic therapy

in patients with advanced, incurable head and neck cancer: a multi-center study. *Head Neck* **32**, 1597–1604.

25. Civantos, F. J., B. Karakullukcu, M. Biel, C. E. Silver, A. Rinaldo, N. F. Saba, R. P. Takes, V. Vander Poorten and A. Ferlito (2018) A review of photodynamic therapy for neoplasms of the head and neck. *Adv. Ther.* **35**, 324–340.

26. Abrahamse, H. and M. R. Hamblin (2016) New photosensitizers for photodynamic therapy. *Biochem. J.* **473**, 347–364.

27. Concu, R. and M. N. D. S. Cordeiro (2018) Cetuximab and the head and neck squamous cell cancer. *Curr. Top. Med. Chem.* **18**, 192–198.

28. Sokolov, V. V., V. I. Chissov, R. L. Yakubovskaya, E. I. Aristarkhova, E. V. Filonenko, T. A. Belous, G. N. Vorozhtsov, N. N. Zharkova, V. V. Smirnov and M. B. Zhitkova (1996) Photodynamic therapy (PDT) of malignant tumours by photosensitzer photosens: results of 45 clinical cases. *SPIE* **2625**, 281–287.

29. Heukers, R., P. M. P. van Bergen en Henegouwen and S. Oliveira (2014) Nanobody-photosensitizer conjugates for targeted photodynamic therapy. *Nanomedicine* **10**, 1441–1451.

30. Kobayashi, H. and P. L. Choyke (2019) Near-infrared photoimmunotherapy of cancer. *Acc. Chem. Res.* **52**, 2332–2339.

31. Mitsunaga, M., M. Ogawa, N. Kosaka, L. T. Rosenblum, P. L. Choyke and H. Kobayashi (2011) Cancer cell-selective in vivo near infrared photoimmunotherapy targeting specific membrane molecules. *Nat. Med.* **17**, 1685–1691.

32. Hartmans, E., M. D. Linssen, C. Sikkens, A. Levens, M. J. H. Witjes, G. M. van Dam and W. B. Nagengast (2017) Tyrosine kinase inhibitor induced growth factor receptor upregulation enhances the efficacy of near-infrared targeted photodynamic therapy in esophageal adenocarcinoma cell lines. *Oncotarget* **8**, 29846–29856.

33. Gillenwater, A. M., D. Cognetti, J. M. Johnson, J. Curry, S. T. Kochuparambil, D. McDonald, M. J. Fidler, K. Stenson, N. Vasan, M. Razaq, J. Campana and F. Mott (2018) RM-1929 photo-immunotherapy in patients with recurrent head and neck cancer: Results of a multicenter phase 2a open-label clinical trial. *J. Clin. Oncol.* **36**(15_suppl), 6039–6039.

34. Palmer, G. M., A. N. Fontanella, S. Shan, G. Hanna, G. Zhang, C. L. Fraser and M. W. Dewhirst (2011) In vivo optical molecular imaging and analysis in mice using dorsal window chamber models applied to hypoxia, vasculature and fluorescent reporters. *Nat. Protocols* **6**, 1355–1366.

35. Ellenbroek, S. I. and J. van Rheenen (2014) Imaging hallmarks of cancer in living mice. *Nat. Rev. Cancer* **14**, 406–418.

36. Seynhaeve, A. L. B. and T. L. M. ten Hagen (2018) Intravital microscopy of tumour-associated vasculature using advanced dorsal skin-fold window chambers on transgenic fluorescent mice. *J. Vis. Exp.* **131**. https://doi.org/10.3791/55115

37. Yokoi, T., A. Yamaguchi, T. Odajima and K. Furukawa (1988) Establishment and characterization of a human cell line derived from a squamous cell carcinoma of the tongue. *Tumour Res.* **23**, 43–57.

38. van Driel, P. B., J. R. van der Vorst, F. P. Verbeek, S. Oliveira, T. J. Snoeks, S. Keereweer, B. Chan, M. C. Boonstra, J. V. Frangioni, P. M. van Bergen en Henegouwen, A. L. Vahrmeijer and C. W. Lowik (2014) Intraoperative fluorescence delineation of head and neck cancer with a fluorescent anti-epidermal growth factor receptor nanobody. *Int. J. Cancer* **134**, 2663–2673.

39. Seynhaeve, A. L., S. Hoving, D. Schipper, C. E. Vermeulen, G. A. de Wiel-Ambagtsheer, S. T. van Tiel, A. M. Eggermont and T. L. Ten Hagen (2007) Tumour necrosis factor alpha mediates homogeneous distribution of liposomes in murine melanoma that contributes to a better tumour response. *Cancer Res.* **67**, 9455–9462.

40. Dou, X., T. Nomoto, H. Takemoto, M. Matsui, K. Tomoda and N. Nishiyama (2018). Effect of multiple cyclic RGD peptides on tumour accumulation and intratumoural distribution of IRDye 700DX-conjugated polymers. *Sci. Rep.* **8**, 8126.

41. Pearson, K. (1896) Mathematical contributions to the theory of evolution III. Regression, heredity and panmixia. *Philos. Trans. R. Soc. London Ser. B* **187**, 253–318.

42. Manders, E. M., J. Stap, G. J. Brakenhoff, R. van Driel and J. A. Aten (1992) Dynamics of three-dimensional replication patterns during the S-phase, analysed by double labelling of DNA and confocal microscopy. *J. Cell Sci.* **103**, 857–862.

43. Manders, E., F. Verbeek and J. Aten (1993) Measurement of colocalization of objects in dual-color confocal images. *J. Microsc.* **169**, 375–382.

44. Star, W. M., H. P. A. Marijnissen, A. E. van den Berg-Blok, J. A. C. Versteeg, K. A. P. Franken and H. S. Reinhold (1986) Destruction of rat mammary tumour and normal tissue microcirculation by hematoporphyrin derivative photoradiation observed in vivo in sandwich observation chambers. *Cancer Res.* **46**, 2532–2540.

45. Chandhuri, K., R. W. Keck and S. Selman (1987) Morphological changes of tumour microvasculature following hematoporphyrin derivative sensitizer photodynamic therapy. *Photochem. Photobiol.* **46**, 823–827.

46. Fingar, V. H., T. J. Wieman, S. A. Wiehle and P. B. Cerrito (1992) The role of microvascular damage in photodynamic therapy: the effect of treatment on vessel constriction, permeability, and leukocyte adhesion. *Cancer Res.* **52**, 4914–4921.

47. Reed, M. W. R., T. J. Wieman, K. W. Doak, K. Pietsch and D. A. Schuschke (1989) The microvascular effects of photodynamic therapy: evidence for a possible role of cyclooxygenase products. *Photochem. Photobiol.* **50**, 419–423.

48. Kerdel, F. A., N. A. Soter and H. W. Lim (1987) In vivo mediator release and degranulation of mast cells in hematoporphyrin derivative-induced phototoxicity in mice. *J. Invest. Dermatol.* **88**, 277–280.

49. Nelson, J. S., L. H. Liaw, A. Orenstein, W. G. Roberts and M. W. Berns (1988) Mechanism of tumour destruction following photodynamic therapy with hematorphyrin derivative, chlorin and phthalocyanine. *J. Natl. Cancer Inst.* **80**, 1599–1605.

50. Agarwal, M. L., M. E. Clay, E. J. Harvey, H. H. Evanes, A. R. Antunez and N. L. Oleinick (1991) Photodynamic therapy induces rapid cell death by apoptosis in L5178Y mouse lymphoma cells. *Cancer Res.* **51**, 5993–5996.